



Effect of Zr doping on the structural and electrical properties of spray deposited TiO₂ thin films

Abayomi T. Oluwabi^{a*}, Albert O. Juma^b, Ilona Oja Acik^a, Arvo Mere^a, and Malle Krunk^a

^a Laboratory of Thin Film Chemical Technologies, Department of Materials Science, Tallinn University of Technology, Ehitajate tee 5, 19086 Tallinn, Estonia

^b Department of Physics and Astronomy, Botswana International University of Science and Technology, Private bag 16, Palapye, Botswana

Received 19 October 2017, revised 19 December 2017, accepted 20 December 2017, available online 5 April 2018

© 2018 Authors. This is an Open Access article distributed under the terms and conditions of the Creative Commons Attribution-NonCommercial 4.0 International License (<http://creativecommons.org/licenses/by-nc/4.0/>).

Abstract. Doping is an effective material re-engineering technique, which provides a possibility of improving properties of materials for different applications. Herein, a Zr-doped TiO₂ thin film was deposited applying the chemical spray pyrolysis method and the influence of varying zirconium dopant concentrations on the properties of the film was studied. Morphological studies showed that the Zr–TiO₂ films were homogeneous with smaller grain sizes compared to the undoped TiO₂ films. As-deposited Zr–TiO₂ films were amorphous while the undoped TiO₂ films were crystalline with anatase structure as revealed by both X-ray diffraction and Raman spectroscopy studies. The optical band gap of the Zr–TiO₂ film was higher (3.44 eV) than that of the undoped TiO₂ films (3.13 eV) showing a strong dependence on the phase composition. As revealed by energy dispersive spectroscopy analysis, the Zr/Ti ratio in the film increased from 0.014 to 0.13 as the doping concentration in the spray solution was increased from 5 to 40 mol%. The current–voltage (I–V) characteristic revealed a reduction of the leakage current in the Zr-doped TiO₂ film (6.06×10^{-5} A) compared to the undoped TiO₂ films (1.69×10^{-3} A) at 1 forward bias voltage. The dielectric relaxation response at the oxide–electrode interface dipole was strongly influenced by the Zr doping concentration in the film.

Key words: chemical spray pyrolysis, doping, thin films, dielectric relaxation, Zr–TiO₂.

1. INTRODUCTION

Recently, silicon-based materials have been in limited use because of the growing interest in cost-effective and low-temperature processing materials that could for example replace the SiO₂ gate dielectric layer of most conventional thin film transistor (TFT) devices [1]. However, solution-processed metal oxide materials such as titanium oxide (TiO₂), zirconium oxide (ZrO₂), hafnium oxide (HfO₂), aluminium oxide (Al₂O₃), tantalum oxide (Ta₂O₅), and their mixtures are tenable alternatives due

to their demonstrated uniformity over a large area and a suitable dielectric constant [1,2].

Titanium oxide and its polymorphs have attractive and promising unique properties ranging from optical to electronic properties, hence it has gained its use in a wide range of applications, especially in TFTs [3–7]. Many routes have been adopted to enhance its properties, but the doping of TiO₂ with different metallic or non-metallic elements has displayed its effectiveness [8,9] owing to the fact that doping affects the phase transition temperature [10] and it can be easily harnessed by controlling the composition of mixed oxides [8].

* Corresponding author, abayomioluwabi@gmail.com

The Zr doping in TiO_2 is chosen because Zr and Ti are isovalent, which supports adequate incorporation of Zr into the TiO_2 lattice thereby increasing its bond length to form a solid solution of $\text{Ti}_{1-x}\text{Zr}_x\text{O}_2$ and stabilizing the anatase phase by delaying crystallite growth [8,11]. In the microstructure of the film formed from the mixture of TiO_2 and ZrO_2 , whose band gap (5.8 eV) and ionic radius (0.084 nm) are higher than those of TiO_2 (band gap 3.0–3.4 eV and ionic radius 0.061 nm), plays an important role [1,8]. Owing to these remarkable properties, different research groups have reported Zr-doped TiO_2 thin films, nanorods, and microspheres for different applications [12,13]. Lukáč et al. [14] reported the effect of the annealing temperature on the photo-catalytic performance of Zr-doped TiO_2 films. Wang's research group [15] investigated the behaviour of Zr^{4+} dopant ion in Zr-doped TiO_2 nanoparticles.

Several methods such as chemical vapour deposition, the sol–gel method, reactive sputtering, and ultrasonic spray pyrolysis have been used to deposit Zr-doped TiO_2 films ([11] and references therein). Among these methods, chemical spray pyrolysis (CSP) is an attractive technique for the preparation of thin films because it is simple to operate and use, film thickness and deposition parameters are easy to control, it can be operated at moderate temperatures, it does not require vacuum, and it is not selective in the choice of substrate [11]. This technique offers an opportunity to deposit uniform and compact films for a wide area of device applications, while the film properties strongly depend on the precursor reagent and on the deposition conditions [16]. Castañeda et al. [17] reported deposition of TiO_2 thin films by spray pyrolysis in the substrate temperature range of 300–500 °C. Okuya et al. [18] also reported the influence of additives in the precursor solution on the mechanism of the crystallization of TiO_2 . The properties of TiO_2 films prepared by the spray pyrolysis method are also reported in [6]. To the best of our knowledge, the properties of Zr-doped TiO_2 thin films deposited by CSP have not been completely studied.

In our study, Zr-doped TiO_2 thin films were deposited using CSP by varying the Zr/Ti mole ratio in the solution. The structural, morphological, optical, and electrical properties of the deposited films were investigated for their application as the dielectric layer in a TFT.

2. EXPERIMENTAL

The Zr-doped TiO_2 films were deposited from analytical-grade titanium(IV) isopropoxide (TTIP) and zirconium acetylacetonate ($\text{Zr}(\text{AcacH})_4$) reagents (from MERCK and ALDRICH, respectively) as the precursors. The synthesis of the TiO_2 precursor was performed as follows: TTIP (1.8 mL) was stabilized with acetylacetonate

(1.2 mL) in the ratio 1 : 2, which was maintained all through the experiment. To this solution, 13.5 mL of ethanol was added and the solution was stirred to ensure homogeneity. The prepared solution was sprayed onto preheated quartz and silicon substrates using a pneumatic spray set-up. The films deposited on the quartz substrate were used for structural studies, while the films deposited on the silicon substrate were used for electrical studies.

The Zr-doped TiO_2 solution was prepared by adding quantitative amounts of $\text{Zr}(\text{AcacH})_4$ corresponding to Zr/Ti mole ratios of 5, 10, 20, and 40 mol% into an already stabilized TTIP and the above procedure was repeated. The substrates were placed on a tin bath (T_{Sn}) maintained at 450 °C and the precursors were sprayed at a rate of 2.5 mL/min with compressed air as the carrier gas. The flow rate of the carrier gas was 8 L/min with one spray cycle consisting of 60 s spraying plus 60 s pause. Ten spray cycles were made from each solution. The samples were then annealed in air for one hour at temperatures from 500 °C to 900 °C using a Nabertherm L5/11/06D furnace. The as-deposited and annealed films were labelled 'undoped TiO_2 ' and ' x -Zr- TiO_2 ' for the undoped and doped samples, respectively, where x corresponds to the mol% concentration of Zr in the sprayed solution.

Optical measurements were performed by measuring total transmittance and total reflectance spectra using a Jasco-V670 spectrophotometer equipped with an integrating sphere in the wavelength range 300–800 nm. The X-ray diffraction (XRD) patterns were obtained using a Rigaku Ultima IV diffractometer, which has a silicon line detector and a $\text{Cu } K_\alpha$ radiation source operated at 40 kV and 40 mA. The surface morphology and elemental composition were studied using a ZEISS HR Ultra 55 scanning electron microscope (SEM) with a Bruker energy dispersive spectroscopy (EDS) system ESPRIT 1.8. The acceleration voltage for SEM measurements was 4.0 kV and for EDS, 7.0 kV. Raman spectra were acquired using a micro-Raman spectrometer HORIBA Jobin Yvon Model HR800 with 532 nm laser excitation line, which delivers 5 mW of power at 10 μm laser spot size during measurements. Raman peak analysis was based on Lorentzian fitting. To access the electrical properties of the as-deposited films, we produced a metal-oxide semiconductor (MOS) device by growing gold contact using a Quorum K975X vacuum evaporator on top of the TiO_2 film surface with a contact area of 1.7 mm², giving a Si/ TiO_2 [Zr]/Au structure. The c-Si wafer was contacted through a eutectic indium alloy to ensure ohmic conductivity. The current–voltage and impedance data were obtained using AUTOLAB PGSTAT30/2 and analysed using frequency–response analysis software. A schematic presentation of the investigated MOS structure is given in Fig. 1.

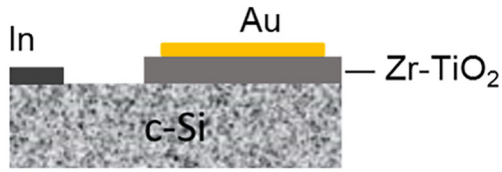


Fig. 1. Metal oxide semiconductor device for measuring electrical properties of x -Zr-TiO₂ thin films ($0 \leq x \leq 40$ mol%).

3. RESULTS AND DISCUSSIONS

3.1. Surface morphology and composition

The SEM images were used to study the influence of varying Zr concentrations in the precursor solution on the morphology of the TiO₂ films. Figure 2 presents the SEM images of the as-deposited ($T_{sn} = 450$ °C) samples and those annealed at 600 and 800 °C. The as-deposited undoped TiO₂ and (5, 20)-Zr-TiO₂ films were uniform and compact. Grains started to increase in the film after annealing at 600 °C (Fig. 2 B, E, H). After annealing at 800 °C the surface of the undoped-TiO₂ film consisted of smaller and larger grains of up to about 250 nm in size (Fig. 2C); however, the surface of the 20-Zr-TiO₂ film (Fig. 2I) consisted of grains with a size of up to about 50 nm.

The thicknesses of films are shown in the insets of Fig. 2. The results obtained revealed that the undoped TiO₂ film was thicker than both 5-Zr-TiO₂ and 20-Zr-TiO₂ films (330 nm, 310 nm, and 250 nm, respectively), which means that the thickness of a film decreased with increasing the Zr concentration in the spray solution. This is a common behaviour of spray deposited doped films [19], which could be due to the fact that increasing the dopant concentration in the solution retards the growth of the film. The film thicknesses in both undoped TiO₂ (322 nm) and 5-Zr-TiO₂ (302 nm) films changed slightly after annealing at 800 °C, but changed significantly in the 20-Zr-TiO₂ film (167 nm). A similar result was reported for zirconium doping by atomic layer deposition [20].

The presence of Zr in the as-deposited Zr-doped TiO₂ film was confirmed by EDS analysis, which revealed an increase in the Zr/Ti atomic ratio in the film from 0 to 0.13 as the mole ratio in the precursor solution was increased from 0 to 40 mol%. The evaluation of Zr content in the film revealed that more than 10% of the Zr content in the precursor solution adequately doped into the film, which indicates that Zr was actually present in the deposited film. This is similar to what was observed for Zr-doped ZnO films deposited by the spray method in [19].

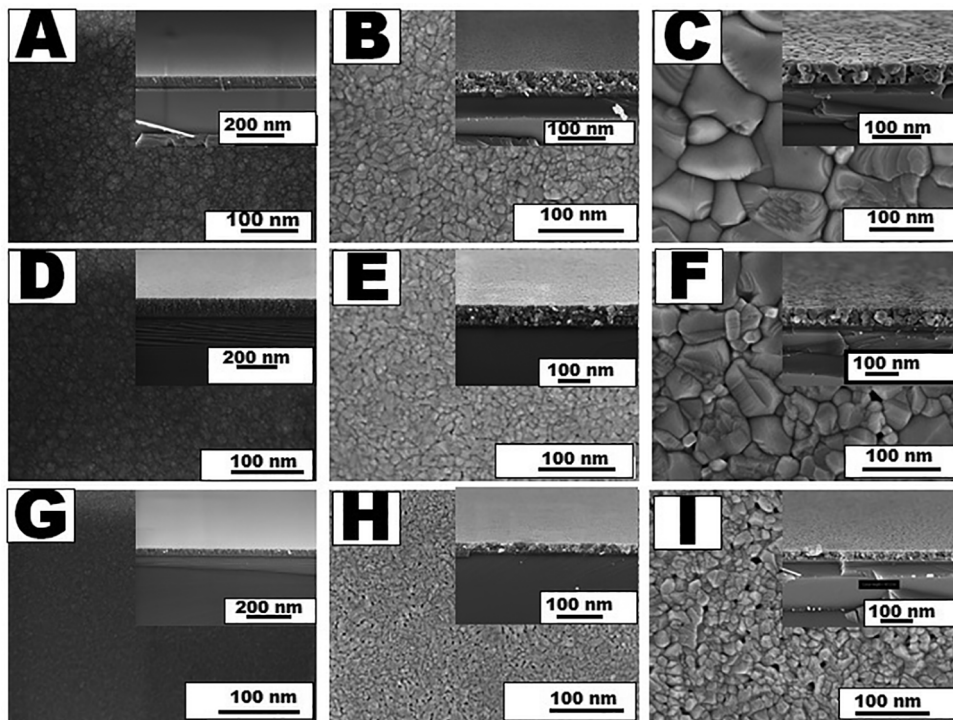


Fig. 2. SEM images of undoped TiO₂ (A–C), 5-Zr-TiO₂ (D–F), 20-Zr-TiO₂ (G–I) thin films; as-deposited (A, D, G) and after annealing at 600 °C (B, E, H) and 800 °C (C, F, I). The inset contains their corresponding SEM cross-sectional images. (Films were deposited on a Si substrate.)

3.2. Structural and phase characterization

3.2.1. XRD study

The obtained XRD patterns of undoped TiO_2 and Zr-doped TiO_2 films are shown in Fig. 3. For the as-deposited samples (Fig. 3a), the undoped TiO_2 film shows a sharp peak and the 5-Zr- TiO_2 film, a weak peak at $2\theta = 25.40^\circ$ belonging to the anatase (101) phase (PDF powder diffraction-01-075-1573). The (10, 40)-Zr- TiO_2 films were amorphous, which indicates an amorphization effect of incorporating Zr into the TiO_2 lattice structure. Gao et al. also reported that Zr doping delays the transition of the amorphous to the anatase phase of TiO_2 deposited by the sol-gel method [21].

The (5, 40)-Zr- TiO_2 films showed amorphous to anatase phase transition after annealing at 500°C , which was sustained up to 700°C . After annealing at 700°C and 800°C (Fig. 3b and c), the undoped TiO_2 film showed a mixture of both rutile and anatase phases

with the anatase (101) peak at $2\theta = 25.40^\circ$ and the rutile (110) main peak at $2\theta = 27.43^\circ$ (PDF01-0714808) while the doped films remained anatase. However, anatase and rutile mixed phases appeared in the 10-Zr- TiO_2 film after annealing at 800°C , which is an indication of the stabilization of the anatase phase thereby delaying the formation of the rutile phase. A similar result on the formation of anatase and rutile mixed phases was also reported by research groups of Schiller et al. and Wang et al. on sol-gel deposited Zr-doped TiO_2 powders and films, respectively [8,15].

Figure 3d reveals the shift in the position of the anatase (101) main peak as a function of the Zr concentration in the solution after annealing at 500°C . The position of the (101) diffraction peak shifted to lower values of the diffraction angle 2θ (from 25.79° to 25.60°) in the diffraction pattern with the increasing Zr amount in the film, which confirms the incorporation of Zr^{4+} in the TiO_2 lattice structure. The presence of Zr^{4+} , which

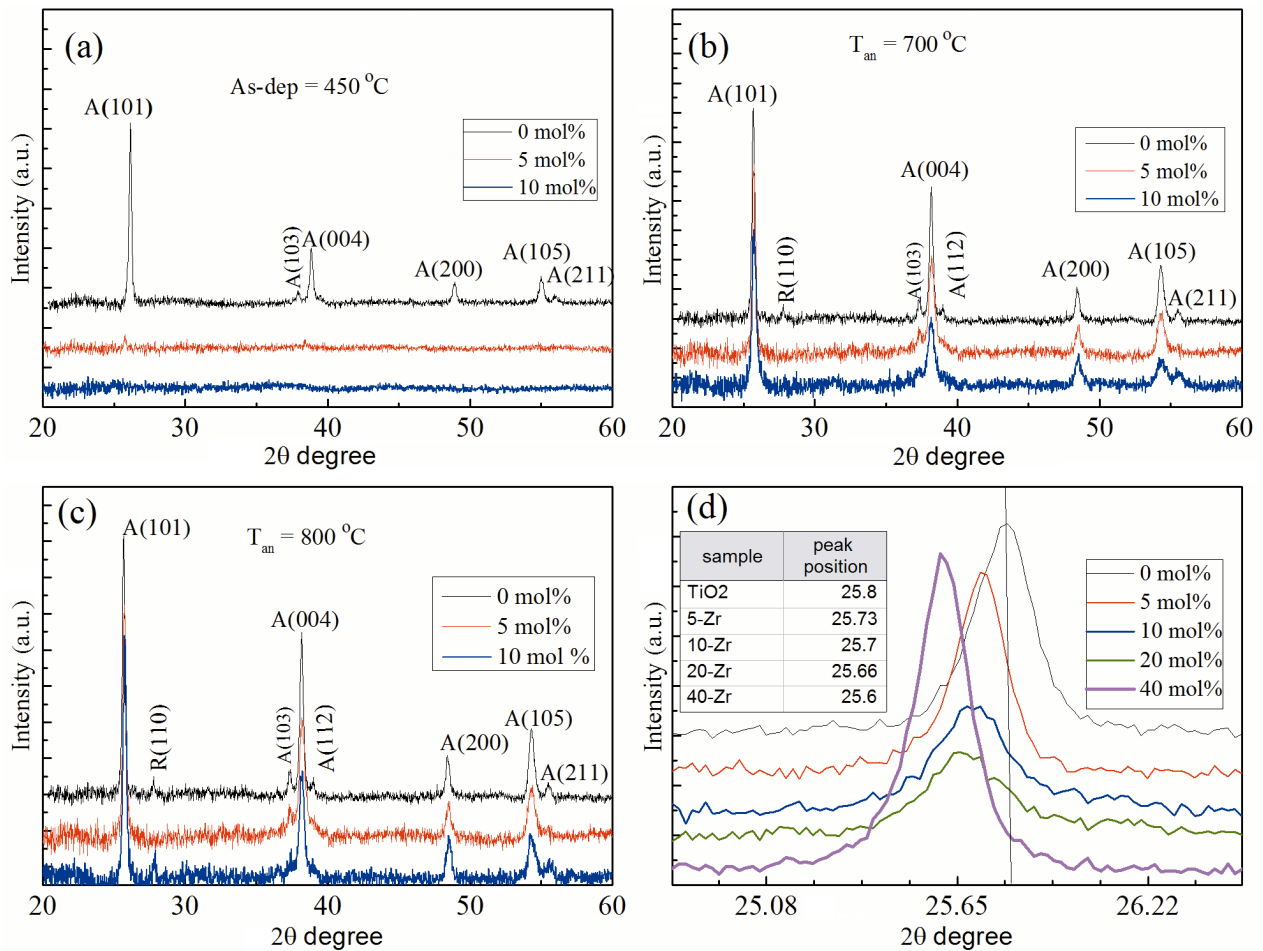


Fig. 3. XRD patterns of undoped and $x\text{-Zr-TiO}_2$ films where $x = 0, 5, 10$ mol%: (a) as-deposited at 450°C , (b) after annealing at 700°C , and (c) 800°C . The shift in the anatase (101) main diffraction peak position (P.P) as a function of the Zr/Ti mole ratio in the spray solution is presented in (d) after annealing at 500°C . (Films were deposited on a quartz substrate.)

has a larger ionic radius of 0.072 nm compared to Ti⁴⁺ (0.061 nm) in the TiO₂ matrix, causes an increase in the unit cell parameters, which brings about a shift in the peak position to a lower 2θ angle as explained by Bragg's law [21].

The mean crystallite size of the undoped TiO₂ and Zr-doped TiO₂ films annealed at different temperatures was calculated by applying the Scherrer formula on the (101) anatase peak; the values obtained are presented in Table 1. The Zr-doped TiO₂ films have smaller mean crystallite sizes than the undoped TiO₂ films, which decrease with an increase in the Zr concentration in the film. At temperatures above 700 °C, the Zr-doped samples displayed distinctively smaller crystallite sizes than the undoped TiO₂ sample, which is an indication of increased amorphization due to Zr doping. This phenomenon is explained by the increase in the number of nucleation sites that inhibit the growth of larger crystallites with doping [8,22,23].

Table 1. Mean crystallite size of undoped TiO₂, 5-Zr-TiO₂, and 20-Zr-TiO₂ films calculated by applying Scherrer's formula on the anatase (101) peak at different temperatures of annealing

Annealing <i>T</i> (°C)	Mean crystallite size, nm		
	TiO ₂	5-Zr-TiO ₂	20-Zr-TiO ₂
500	40	50	30
600	30	30	20
700	35	30	25
800	40	35	30
1000	50	45	40

3.2.2. Raman study

The Raman spectra for the undoped and Zr-doped TiO₂ films are shown in Fig. 4. The as-deposited TiO₂ spectrum reveals a Raman band at 141 cm⁻¹ belonging to the TiO₂

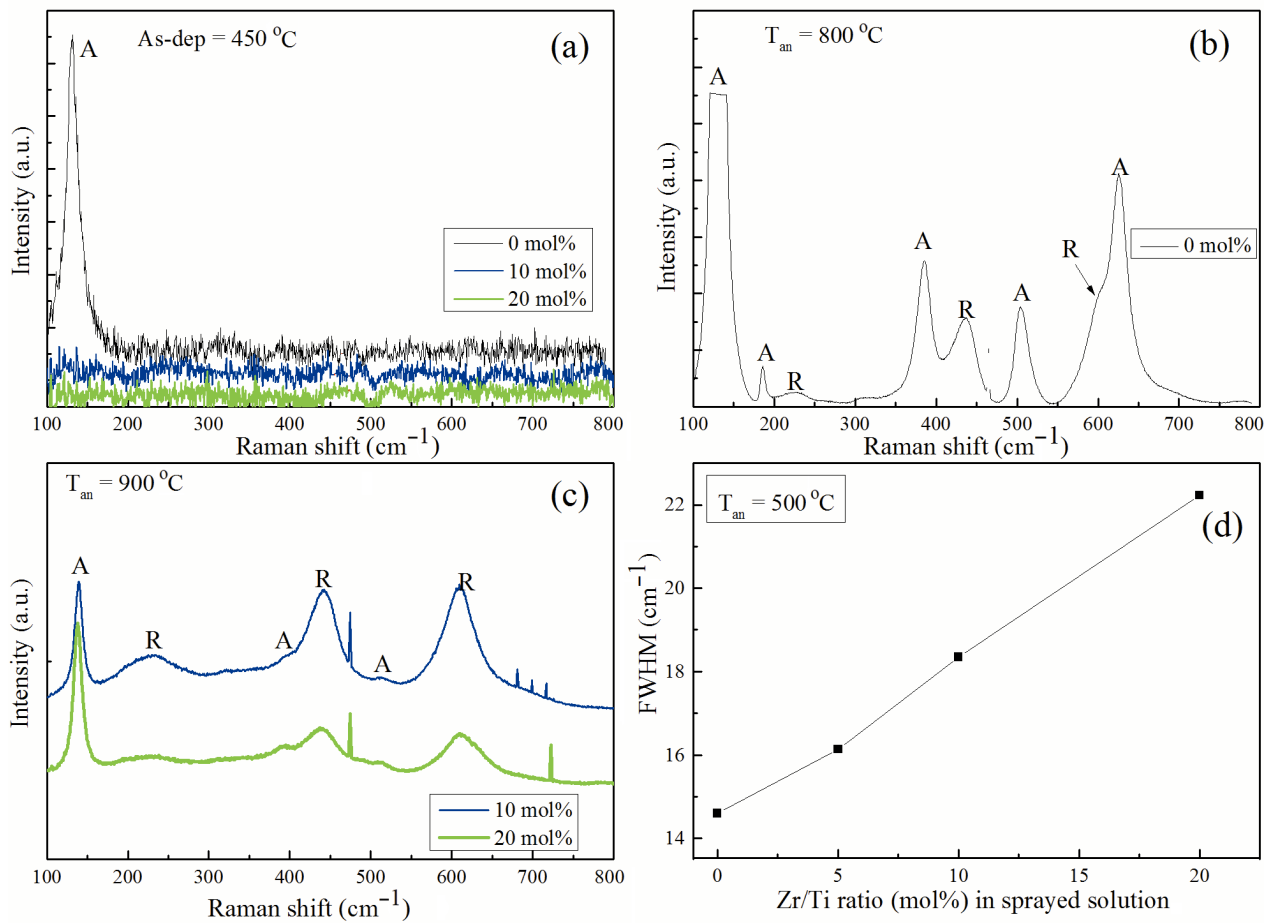


Fig. 4. Raman spectra of the as-deposited undoped and (10, 20)-Zr-TiO₂ films grown at 450 °C (a), undoped TiO₂ film after annealing at 800 °C (b), and (10, 20)-Zr-TiO₂ films after annealing at 900 °C (c). The FWHM as a function of Zr/Ti mol ratio in the spray solution after annealing at 500 °C is presented in (d). (Films were deposited on a quartz substrate.)

denotes an increase in the optical band gap with an increasing Zr concentration caused by a change of the lattice constant.

The optical direct band gap energy of the deposited films was calculated by applying expression (1) on a Tauc plot [29] after taking into consideration the reflectivity, absorption coefficient, and film thickness as these strongly affect the transparency of the film.

$$(\alpha h\nu) = A(h\nu - E_g)^n. \quad (1)$$

Here α is the optical absorption coefficient, $h\nu$ is the photon energy, A is a constant called critical absorption, the value of n varies depending on whether the band transition is direct or indirect, and E_g is the optical band gap. The values of E_g for undoped and Zr-doped TiO₂ films were obtained by plotting $(\alpha h\nu)^{1/n}$ against the photon energy ($h\nu$) when the value of $n = 0.5$ for direct transition. The linear part of the curve was then extrapolated to the $h\nu$ axis as shown in Fig. 6a for (0-10)-Zr-TiO₂ films [30,31]. The band gap energy of the 10-Zr-TiO₂ thin film (3.2 eV) was higher than that of the undoped TiO₂ film (3.14 eV). The value of E_g increased slightly (from 3.23 eV to 3.38 eV) with annealing temperature rising up to 600–700 °C and later decreased (to 3.05 eV) as the rutile phase started to form in the 10-Zr-TiO₂ thin film (Fig. 6b).

Theoretical calculations of the electronic properties of Zr-doped TiO₂ films show no change in the band gap [32,33] while experiments have given mixed results depending on the method of the preparation and the nature of doping. An increase in the band gap was reported for nanocrystalline samples, which was attributed to the quantum confinement effect because of the small particle sizes [34]. The increase in the band gap and

decreased crystallite sizes with Zr-doping were reported for sol-gel deposited samples [17,28]. The slight change in the band gap values observed in this work can therefore be due to structural changes caused by Zr-doping and annealing [14].

3.4. Electrical studies

3.4.1. Current-voltage characteristics

The leakage current in the forward bias regime is illustrated in Fig. 7 for the as-deposited undoped TiO₂ and (20, 40)-Zr-TiO₂ films. The leakage current at 1 V amounted to 1.7×10^{-3} A, 6.1×10^{-5} A, and 4.5×10^{-5} A for undoped-TiO₂, 20-Zr-TiO₂, and 40-Zr-TiO₂, respectively. The Zr dopant helped to reduce the leakage current by two orders of magnitude. Considering the fact that the leakage current is exponentially dependent on the thickness of the insulating layer, we normalized the thickness value in both undoped TiO₂ and Zr-doped TiO₂ layers to 200 nm in our calculations. This helped us to prove that the tendency we show in Fig. 7 was due to the dopant effect. For TiO₂ deposited by the CSP technique, leakage currents of similar magnitudes were reported in the literature [35]. The zero-bias barrier heights of the undoped and Zr-doped TiO₂ samples were determined from the vertical intercept of the $\ln(I)$ - V plots (plot not shown) and calculated using the following expression [36]:

$$\Phi_B = \frac{kT}{q} \ln \left(\frac{AA^*T^2}{I_0} \right), \quad (2)$$

where A is the effective area of the diode, A^* is the effective Richardson constant equal to $1200 \text{ A cm}^{-2} \text{ T}^{-2}$

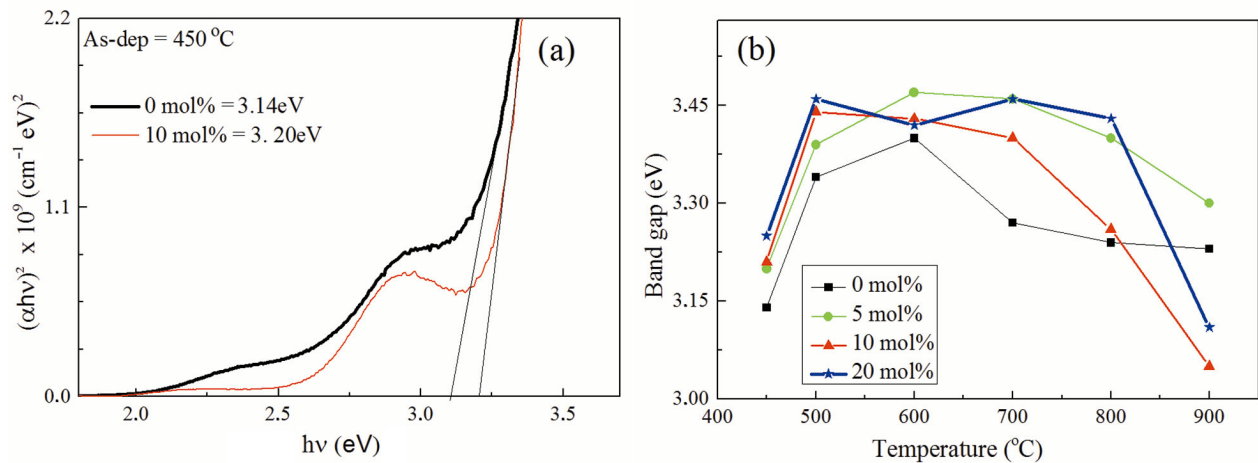


Fig. 6. (a) Determination of the optical band gap of as-deposited undoped and Zr-doped TiO₂ films and (b) the variation of the band gap of the undoped and Zr-doped TiO₂ films with the annealing temperature. (Films were deposited on a quartz substrate.)

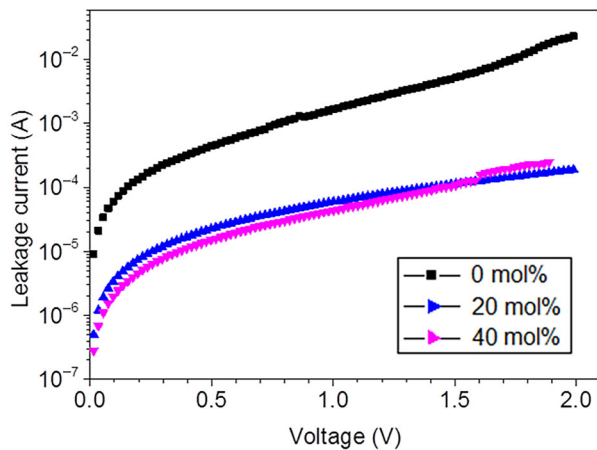


Fig. 7. Leakage current as a function of forward bias voltage for x -Zr-TiO₂ films where the concentration of Zr in the solution $x = 0, 20,$ and 40 mol%. The metal oxide semiconductor structure is Si/TiO₂[Zr]/Au.

for TiO₂ [37], k is the Boltzmann constant, and Φ_B is the Schottky barrier height.

The reverse saturation current I_0 amounted to 8.45×10^{-3} A/cm², 3.84×10^{-3} A/cm², and 2.53×10^{-3} A/cm² for the undoped TiO₂, 20-Zr-TiO₂, and 40-Zr-TiO₂, respectively. The values of Φ_B obtained using Eq. (2) amounted to 0.536, 0.562, and 0.571 eV for the undoped TiO₂, 20-Zr-TiO₂, and 40-Zr-TiO₂, respectively. The decrease in the leakage current observed could be due to the possibility of the material losing its conductivity in the forward regime. These values compare well with those found in the literature for similar structures of TiO₂ deposited by other methods such as spray pyrolysis [35],

magnetron sputtering [38], plasma enhanced physical vapour deposition [39], and dip coating [40], for which Schottky barrier heights between 0.4 and 1.0 eV were reported. It is evident that the electronic properties of TiO₂ thin films and their derivatives depend strongly on the deposition method and conditions.

3.4.2. Frequency response analysis

Figure 8a shows the Nyquist plot for the as-deposited undoped TiO₂ and Zr-doped TiO₂ thin films on Si substrates. The plots from the undoped TiO₂ and 20-Zr-TiO₂ with Zr/Ti = 20 mol% were multiplied by a factor of 50 for better presentation and comparison. The Nyquist plot for the undoped TiO₂ film shows more than one semicircle, implying that the sample could be modelled by more than one parallel resistor–capacitor (RC) circuit combination. For the (20, 40)-Zr-TiO₂ films, it appears that the semicircles enlarge and overlap to form a larger semicircle. The increase in the Z' component is much greater than that in the Z'' component, indicating a strong increase in the parallel resistance compared to the change in the capacitance of the TiO₂ with doping.

In Fig. 8b a slight increase in the total impedance for the 20-Zr-TiO₂ sample and a strong increase in the 40-Zr-TiO₂ sample by almost two orders of magnitude can be observed. The undoped-TiO₂ sample shows two points of inflection (where the gradient changes) at frequencies of 4 kHz and 110 kHz, while the doped samples have inflection points at 42 kHz and 620 Hz for the 20-Zr-TiO₂ and 40-Zr-TiO₂ samples, respectively. The Bode phase plots show phase angles close to 90° in

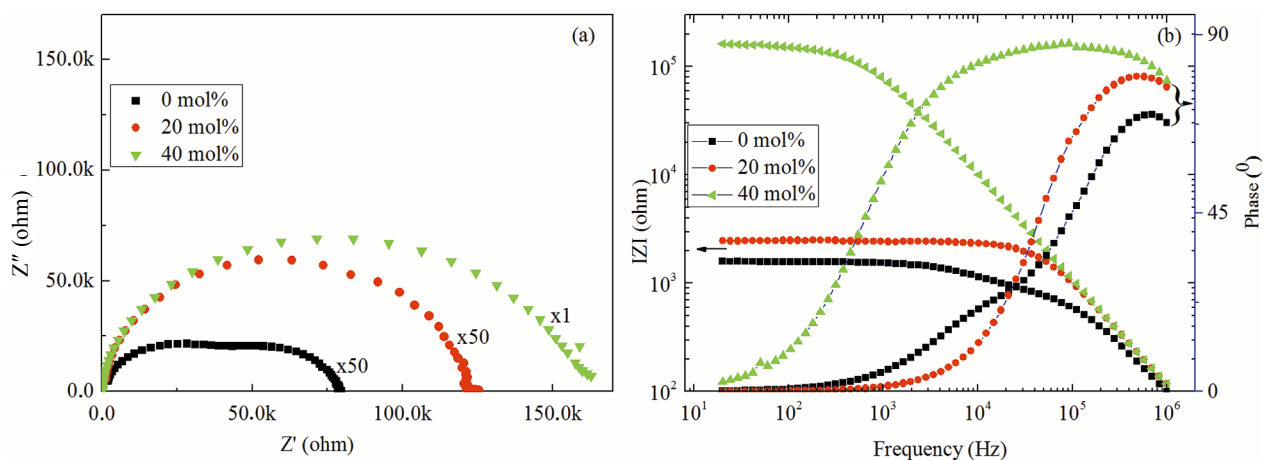


Fig. 8. Nyquist plot (a) and Bode plot (b) for the x -Zr-TiO₂ film where the concentrations of Zr in the solution $x = 0, 20,$ and 40 mol%. The impedance plots for the TiO₂ and 20-Zr-TiO₂ samples were multiplied by a factor of 50 for the purpose of comparison. The metal oxide semiconductor structure is Si/TiO₂[Zr]/Au.

the high frequency region, exhibiting more capacitive behaviour, but in the low frequency region, the phase is close to zero. The undoped TiO₂ film shows two peaks in the mid- and high-frequency regions. However, the (20, 40)-Zr-TiO₂ films show one broad peak spanning the mid- and high-frequency regions, which broadens as the amount of Zr dopant in the film increases from 20 to 40 mol%.

By plotting Z' vs $\omega Z''$ as proposed by Abrantes et al. [41] and Walke et al. [42], the contributions from different relaxation frequencies that correspond to the circuit time constant can be resolved. The relaxation frequencies are determined from the slopes of the linear sections of the Z' vs $\omega Z''$ plots as demonstrated in Fig. 9. The undoped TiO₂ film shows three different slopes resulting in three relaxation frequencies of 72 kHz, 6 kHz, and 650 Hz. Based on this result, the undoped TiO₂ film can be accurately represented by an equivalent circuit composed of three parallel RC components. The 20-Zr-TiO₂ film shows only two slopes of relaxation frequencies 47 kHz and 30 kHz, which are quite close. The 40-Zr-TiO₂ film shows three slopes with relaxation frequencies 750 Hz, 540 Hz, and 186 Hz. It was observed that as the concentration of the dopant was increased, the relaxation frequency shifted to much lower frequencies. This implies that with higher Zr doping the dielectric response due to the oxide-electrode interface dipoles dominates the dielectric properties of the Si/Zr-TiO₂/Au structure [43]. Understanding the nature of such interfaces as a function of the dopant type and concentration is therefore crucial to the performance of any electronic devices.

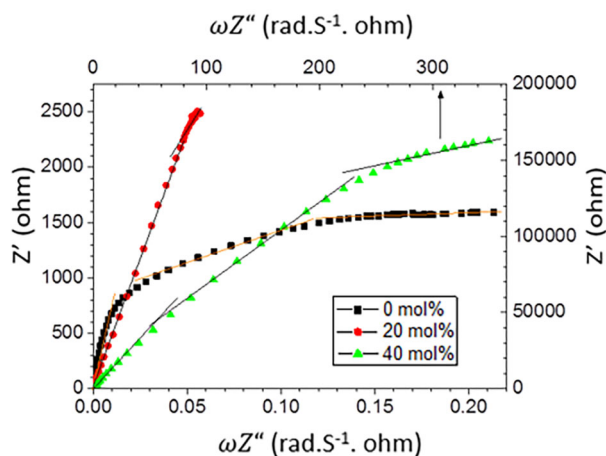


Fig. 9. Real part of the impedance vs imaginary part divided by the frequency for x -Zr-TiO₂ films where the concentrations of Zr in the solution $x = 0, 20$, and 40 mol%. The scale for the 40-Zr-TiO₂ film sample is top and right. The metal oxide semiconductor structure is Si/TiO₂[Zr]/Au.

4. CONCLUSIONS

The CSP method was successfully used to deposit a uniform and homogeneous Zr-doped TiO₂ film. The XRD data reveal that the as-deposited Zr-doped TiO₂ samples were amorphous, which became crystalline with anatase crystal structure after annealing at 500 °C. The average crystallite sizes were between 20 and 50 nm. A mixture of anatase and rutile phases was observed for the Zr-doped TiO₂ after annealing at 800 °C. Raman analysis, which complements the XRD results, showed that the FWHM value of the anatase main peak at 141 cm⁻¹ increased with Zr/Ti mole ratio in the precursor solution, confirming the decrease in the crystallite sizes with enhanced Zr doping. The leakage current in the as-deposited TiO₂ was reduced by two orders of magnitude with Zr doping of TiO₂ and the dielectric relaxation response at the oxide-electrode interface shifted to lower frequencies, from 72 kHz to 750 Hz, as the Zr concentration in the sprayed solution was increased, thus influencing the dielectric properties of the Si/Zr-TiO₂/Au structure. The results indicated that Zr dopant influenced the properties of CSP deposited TiO₂ films, being compatibly useful as the gate dielectric layer in the transistor application of thin film.

ACKNOWLEDGEMENTS

The authors acknowledge V. Mikli for SEM and EDS measurements. This study was financially supported by the Estonian Ministry of Education and Research, project IUT19-4, Tallinn University of Technology based financing project B24, and by the European Union through the European Regional Development Fund project TK141 'Advanced materials and high-technology devices for energy recuperation systems'. The publication costs of this article were covered by the Estonian Academy of Sciences.

REFERENCES

1. Barquinha, P., Martins, R., Pereira, L., and Fortunato, E. *Transparent Oxide Electronics*. John Wiley and Sons, United Kingdom, 2012.
2. Bengi, A., Aydemir, U., Altındal, Ş., Özen, Y., and Özçelik, S. A comparative study on the electrical characteristics of Au/n-Si structures with anatase and rutile phase TiO₂ interfacial insulator layer. *J. Alloys Comp.*, 2010, **505**, 628–633.
3. Lee, M-K., Yen, C-F., and Fan, C-H. High dielectric constant of nickel-doped titanium oxide films prepared by liquid-phase deposition, *Appl. Phys. A*, 2014, **116**, 2007–2010.

4. Frank, A. J., Kopidakis, N., and van de Lagemaat, J. Electrons in nanostructured TiO₂ solar cell: transport recombination and photovoltaic properties. *Coord. Chem. Rev.*, 2004, **248**, 1165–1179.
5. Kim, S. K., Kim, K. M., Jeong, D. S., Jeon, W., Yoon, K. J., and Hwang, C. S. Titanium dioxide thin films for next generation memory devices. *J. Mater. Res.*, 2013, **28**, 313–325.
6. Es-Souni, M., Oja, I., and Krunk, M. Chemical solution deposition of thin TiO₂-anatase films for dielectric application. *J. Mater. Sci. – Mater. El.*, 2004, **15**, 341–344.
7. Woebkenberg, P. H., Ishwara, T., Nelson, J., Bradley, D.-D. C., Haque, S. A., and Anthopoulos, T. D. TiO₂ thin film transistor fabricated by spray pyrolysis. *Appl. Phys. Lett.*, 2010, **96**, 082116.
8. Schiller, R., Weiss, C.-K., and Landfester, K. Phase stability and photocatalytic activity of Zr-doped anatase synthesised in miniemulsion. *J. Nanotechnol.*, 2010, **21**, 405603.
9. Liu, G., Yang, H. G., Wang, X., Cheng, L., Pan, J., Lu, G. Q., and Cheng, H. M. Nano sized anatase TiO₂ single crystals for enhanced photocatalytic activity. *J. Am. Chem. Soc.*, 2009, **131**, 12868.
10. Reidy, D. J., Holmes, J. D., and Morris, M. A. The critical size mechanism for the anatase to rutile transformation in TiO₂ and doped-TiO₂. *J. Eur. Ceram. Soc.*, 2006, **26**, 1527–1534.
11. Juma, A., Oja-Acik, I., Oluwabi, A. T., Mere, A., Mikli, V., Danilson, M., and Krunk, M. Zirconium doped TiO₂ thin films deposited by chemical spray pyrolysis. *Appl. Surf. Sci.*, 2016, **387**, 539–545.
12. Hernández-Alonso, M. D., Coronado, J. M., Bachiller-Baeza, B., Fernández-García, M., and Soria, J. Influence of structural and surface characteristics of Ti_{1-x}Zr_xO₂ nanoparticles on the photocatalytic degradation of methylcyclohexane in the gas phase. *Chem. Mater.*, 2007, **19**, 4283–4291.
13. Huang, Y., Zheng, Z., Al, Z., Zhang, L., Fan, X., and Zou, Z. Core shell microspherical Ti-Zr-O₂ solid solution photocatalyst directly from ultrasonic spray pyrolysis. *J. Phys. Chem. B*, 2006, **110**, 19323–19328.
14. Lukáč, J., Klementová, M., Bezdička, P., Bakardjieva, S., Šubrt, J., Szatmáry, L., et al. Influence of Zr as TiO₂ doping on photocatalytic degradation of 4-chlorophenol. *Appl. Catal. B-Environ.*, 2007, **74**, 83–91.
15. Wang, J., Yu, Y., Li, S., Guo, L., Wang, E., and Cao, Y. Doping behaviour of Zr⁴⁺ ions in Zr⁴⁺-doped TiO₂ nanoparticles. *J. Phys. Chem. C*, 2013, **117**, 27120–27126.
16. Patil, P. S. Versatility of chemical spray pyrolysis technique. *Math. Chem. Phys.*, 1999, **59**, 185–198.
17. Castañeda, L., Alonso, J. C., Ortiz, A., Andrade, E., Saniger, J. M., and Banuelos, J. G. Spray pyrolysis deposition and characterization of titanium oxide thin films. *Mater. Chem. Phys.*, 2002, **77**, 938–944.
18. Okuya, M., Prokudina, N. A., Mushika, K., and Kaneko, S. TiO₂ thin film synthesised by spray pyrolysis deposition technique. *J. Eur. Ceram. Soc.*, 1999, **19**, 903–906.
19. Gokulakrishnan, V., Parthiban, S., Jeganathan, K., and Ramamurthi, K. Investigation on the effect of Zr doping in ZnO thin films by spray pyrolysis. *Appl. Surf. Sci.*, 2011, **257**, 9068–9072.
20. Herodotou, S. *Zirconium Doped Zinc Oxide Thin Film Deposited by Atomic Layer*. PhD thesis. The University of Liverpool, 2015. <http://livrepository.liverpool.ac.uk/2013045/201> (accessed 2018-03-12).
21. Gao, B., Lim, T. M., Subagio, D. P., and Lim, T.-T. Zr-doped TiO₂ for enhanced photocatalytic degradation of bisphenol A. *Appl. Catal. A-Gen.*, 2010, **375**, 107–115.
22. Hanaor, D. A. H. and Sorrell, C. C. Review of the anatase to rutile phase transformation. *J. Mater. Sci.*, 2011, **46**, 855–874.
23. Gnatyuk, Yu., Smirnova, N., Korduban, O., and Eremenko, A. Effect of zirconium incorporation on the stabilization of TiO₂ mesoporous structure. *Surf. Interface. Anal.*, 2010, **42**, 1276–1280.
24. Ohsaka, T., Izumi, F., and Fujiki, Y. Raman spectrum of anatase TiO₂. *J. Raman Spectrosc.*, 1978, **7**, 321–324.
25. Zhang, W. F., He, Y. L., Zhang, M. S., Yin, Z., and Chen, Q. Raman scattering study on anatase TiO₂ nanocrystals. *J. Phys. D: Appl. Phys.*, 2000, **33**, 912–916.
26. Bineesh, K. V., Kim, D.-K., and Park, D.-W. Synthesis and characterisation of zirconium-doped mesoporous nano-crystalline TiO₂. *Nanoscale*, 2010, **2**, 1222–1228.
27. Kim, S.-S., Yum, J.-H., and Sung, Y.-E. Flexible dye-sensitized solar cells using ZnO coated TiO₂ nanoparticles. *J. Photochem. Photobiol. A. Chem.*, 2005, **171**, 269–273.
28. Bensaha, R. and Bensouyad, H. Synthesis, characterisation and properties of zirconium oxide (ZrO₂)-doped titanium oxide (TiO₂) thin films obtained via sol-gel process. In *Heat Treatment – Conventional and Novel Applications* (Czervinski, F., ed.). IntechOpen, 2012, chapter **10**, 207–234.
29. Pankove, J. I. *Optical Process in Semiconductors*. Prentice-Hall, Englewood Cliffs, NJ, 1971.
30. Zhao X. K. and Fendler, J. H. Size quantization in semiconductor particulate films. *J. Phys. Chem.*, 1991, **95**, 3716–3721.
31. Tang, H., Prasad, K., Sanjinès, R., Schmid, P. E., and Lévy, F. Electrical and optical properties of TiO₂ anatase thin film. *J. Appl. Phys.*, 1994, **75**, 2042–2204.
32. Yao, X., Wang, X., Su, L., Yan, H., and Yao, M. Band structure and photocatalytic properties of N/Zr co-doped anatase TiO₂ from first-principle study. *J. Mol. Catal. A-Chem.*, 2011, **351**, 11–16.
33. Lippens, P. E., Chadwick, A. V., Weibel, A., Bouchet, R., and Knauth, P. Structure and chemical bonding in Zr-doped anatase TiO₂ nanocrystals. *J. Phys. Chem. C*, 2008, **112**, 43–47.
34. Venkatachalam, N., Palanichamy, M., Arabinthoo, B., and Murugesan, V. Enhanced photocatalytic degradation of 4-chlorophenol by Zr⁴⁺ doped nano TiO₂. *J. Mol. Catal. A-Chem.*, 2007, **266**, 158–165.
35. Juma, A. O., Oja Acik, I., Mere, A., and Krunk, M. Dielectric relaxation and conduction mechanisms in sprayed TiO₂ thin films as a function of the annealing temperature. *Appl. Phys. A-Mater.*, 2016, **122**, 359.

36. Zeyrek, S., Altındal, S., Yüzer, H., and Bülbül, M. M. Current transport mechanism in Al/Si₃N₄/p-Si (MIS) Schottky barrier diodes at low temperatures. *Appl. Surf. Sci.*, 2006, **252**, 2999–3010.
37. Enright, B. and Fitzmaurice, D. Spectroscopic determination of electron and hole effective masses in a nanocrystalline semiconductor film. *J. Phys. Chem.*, 1996, **100**, 1027–1035.
38. Xue, H., Chen, W., Liu, C., Kong, X., Qu, P., Liu, Z., et al. Fabrication of TiO₂ Schottky barrier diodes by RF magnetron sputtering. In *Proceedings of the 3rd IEEE International Conference on Nano/Micro Engineered and Molecular Systems, Sanya, China*, 2008, 108–111.
39. Chakraborty, S., Bera, M. K., Bhattacharya, S., and Maiti, C. K. Current conduction mechanism in TiO₂ gate dielectrics. *Microelectron. Eng.*, 2005, **81**, 188–193.
40. Sönmezoglu, S. and Akin, S. Current transport mechanism of antimony-doped TiO₂ nanoparticles based on MOS device. *Sensor. Actuat. A-Phys.*, 2013, **199**, 18–23.
41. Abrantes, J. C. C., Labrincha, J. A., and Frade, J. R. An alternative representation of impedance spectra of ceramics. *Mater. Res. Bull.*, 2000, **35**, 727–740.
42. Walke, P., Bouregba, R., Lefevre, A., Parat, G., Lallemand, F., Voiron, F., et al. Giant dielectric constant in TiO₂/Al₂O₃ nanolaminates grown on doped silicon substrate by pulsed laser deposition. *J. Appl. Phys.*, 2014, **115**, 094103.
43. Zhao, C., Zhao, C. Z., Werner, M., Taylor, S., and Chalker, P. Dielectric relaxation of high-k oxides. *Nanoscale Res. Lett.*, 2013, **8**, 456.

Zr-legerimise mõju pihustuspürolüüsimeetodil sadestatud TiO₂ õhukeste kilede struktuursetele ja elektrilistele omadustele

Abayomi T. Oluwabi, Albert O. Juma, Ilona Oja Acik, Arvo Mere ja Malle Krunks

Antud uurimistöös sadestati zirkooniumiga legeritud TiO₂ (Zr-TiO₂) kiled keemilisel pihustuspürolüüsimeetodil. Uurimistöö eesmärk oli uurida Zr kui legeriva elemendi mõju pihustatud TiO₂ kilede morfoloogilistele, struktuurilistele, optilistele ja elektrilistele omadustele ning hinnata antud materjali võimekust töötada dielektrilise kihina õhukesekilelistes transistorides. Leiti, et pihustatud Zr-TiO₂ kiledel on väiksem tera suurus kui legerimata TiO₂ kiledel. EDS-analüüs näitas, et Zr/Ti aatomsuhe kiledes suureneb 0,014 kuni 0,13, kui tõsta Zr kontsentratsiooni pihustuslahuses vahemikus 5–40 mol%. XRD- ja Ramani analüüs näitas, et äsja sadestatud TiO₂ kiled on kristallilised anataasi struktuuriga, kuid Zr-TiO₂ kiled on amorfseid. TiO₂ kilede kuumutamisel 700 °C ja Zr-TiO₂ kilede kuumutamisel 800 °C juures saadi kiled, mis koosnesid anataasi ning rutiili faaside segust. TiO₂ ja Zr-TiO₂ kiled näitasid optilist keelutsooni väärtust vastavalt 3,13 ning 3,44 eV. Äsja sadestatud 20-Zr-TiO₂ kiled näitavad rakendatud päripinge 1 V juures väiksemat lekkevoolu ($6,06 \times 10^{-5}$ A) kui TiO₂ kiled ($1,69 \times 10^{-3}$ A). Töö tulemusena leiti, et pihustuspürolüüsimeetodil sadestatud ja järelkuumutatud Zr-TiO₂ kiledel on perspektiivi, kasutamaks neid dielektrilise kihina õhukesekilelistes transistorides.